Skeletal Age Assessment in Children Using an Open Compact MRI System

Yasuhiko Terada,[1]* Saki Kono,[1] Daiki Tamada,[1] Tomomi Uchiumi,[1] Katsumi Kose,[1] Ryo Miyagi,[2] Eiko Yamabe,[2] and Hiroshi Yoshioka[2]

MRI may be a noninvasive and alternative tool for skeletal age assessment in children, although few studies have reported on this topic. In this article, skeletal age was assessed over a wide range of ages using an open, compact MRI optimized for the imaging of a child's hand and wrist, and its validity was evaluated. MR images and their three-dimensional segmentation visualized detailed skeletal features of each bone in the hand and wrist. Skeletal age was then independently scored from the MR images by two raters, according to the Tanner–Whitehouse Japan system. The skeletal age assessed by MR rating demonstrated a strong positive correlation with chronological age. The intrarater and inter-rater reproducibilities were significantly high. These results demonstrate the validity and reliability of skeletal age assessment using MRI. **Magn Reson Med 69:1697–1702, 2013. © 2012 Wiley Periodicals, Inc.**

Key words: open compact MRI; imaging technique; skeletal age assessment; pediatrics

INTRODUCTION

Skeletal age is a standard measure of growth for children and is often determined by assessing skeletal maturity visible in a radiograph (e.g., the appearance of ossification centers and epiphyseal plate fusion; Ref. 1). It is important to evaluate any variables of skeletal maturation in the diagnosis of endocrinological diseases, chronic diseases, hormonal therapy follow-up, and computing height predictions for prognostic and therapeutic purposes (2). The Greulich–Pyle (3) and Tanner–Whitehouse (TW2) (4) systems are the most popular methods based on the evaluation of a left hand and wrist radiograph. In the Greulich–Pyle system, a rater focuses on a number of maturational indicators and matches the hand to one of the reference images in the Greulich–Pyle atlas (3), whereas in the TW2 system, a rater assigns a maturity stage for 20 bones of the hand and wrist in the radiograph. Each stage has a corresponding score of skeletal maturation. The sum of each bone score is transformed into a bone age using standards for a skeletal maturity score (4).

However, standard radiography poses a radiation risk, which cannot be justified as a screening tool for healthy children. The us: and possible abuse of radiation exposure is restricted by the International Atomic Energy Agency under the title "International basic safety standards for protection against ionizing radiation and for safety of radiation sources" (CD-ROM edition, 2003, Geneva, Switzerland), and an alternative method for skeletal age assessment is required.

Many skeletal disorders are currently diagnosed with multiple imaging tools such as ultrasonography, computed tomography, magnetic resonance imaging (MRI), and positron emission tomography. Bilgili et al. reported the accuracy of skeletal age assessment in 97 children up to 6 years of age using ultrasonography of the hand and wrist (5). They demonstrated that the skeletal age derived from the ultrasonography chart showed an excellent correlation with that derived from plain radiography. However, their study only included children younger than 6 years of age, and diagnosis using ultrasonography is generally highly dependent on the operator.

Use of MRI to estimate skeletal age is a novel idea. MRI is noninvasive and nonirradiative and also provides excellent soft-tissue contrast and multiplanar cross-sectional imaging capability. It could be used as an alternative method of skeletal age examination. There have been several studies that assessed the skeletal age of teenagers and determined the degree of the epiphyseal fusion of the radius using MRI (6–8). Dvorak et al. (6) reported that MRI of the wrist offers an alternative method of age determination in 14- to 19-year-old male adolescents using a 1 or 1.5T scanner. However, there has been no report on MR skeletal examination over a wide range of ages. In addition, no one has used a dedicated open extremity scanner for skeletal age assessment. The open, compact MRI offers adequate performance with greater comfort, is less claustrophobic, and is more convenient for children without sedation.

Accordingly, the aim of this study is to assess a wide range of skeletal ages without ionizing radiation on a dedicated open, compact MRI scanner, and to evaluate its validity. Furthermore, this study was performed on a uniform ethnic cohort comprising Japanese descendants (as skeletal ages determined from standard radiographs may vary depending on ethnic origin), which enhanced validity of the skeletal age assessment with MRI.

METHODS

Subjects

A total of 93 healthy Japanese children (age range = 4.1–16.4 years; mean = 9.7 years; 50 boys and 43 girls) were recruited from the local community. Those with a

[1]Institute of Applied Physics, University of Tsukuba, Tsukuba, Ibaraki, Japan.
[2]Department of Radiological Sciences, University of California Irvine, Irvine, California, USA.
*Correspondence to: Yasuhiko Terada, Ph.D., Institute of Applied Physics, University of Tsukuba, Tsukuba, 1-1-1 Tennodai, Tsukuba, Ibaraki 305-8573, Japan. E-mail: terada@bk.tsukuba.ac.jp

Received 30 January 2012; revised 12 June 2012; accepted 5 July 2012.
DOI 10.1002/mrm.24439
Published online 31 July 2012 in Wiley Online Library (wileyonlinelibrary.com).

history of genetic, developmental, metabolic, or endocrinal diseases, or wrist trauma, or who were on medication including hormonal supplements were excluded. Written informed consent was obtained from both the child and one of the parents. All MRI measurements were performed under the approval of the ethical committee of the Graduate School of Pure and Applied Sciences, University of Tsukuba.

MR Measurements

We used an open, compact MRI with a permanent magnet (NEOMAX Engineering, Tokyo, Japan; field strength = 0.3 T; gap = 142 mm; homogeneity = 50 ppm over the 22 × 22 × 8 cm^3 diameter ellipsoidal volume; weight = 700 kg), which was originally developed for whole-hand examination for the diagnosis of rheumatoid arthritis (Fig. 1; Refs. 9 and 10). The same type of scanner was also used elsewhere (11). The radiofrequency coil was a 16-turn solenoid optimized for the imaging of a child's hand and wrist. To minimize voluntary hand motion, each subject sat down in a chair and looked at a television screen (Fig. 1). The subject's hand was fixed onto a plastic plate using a flexible cloth belt as firmly as possible without being painful. A three-dimensional (3D) coherent gradient-echo sequence was used (dwell time = 20 μs; pulse repetition time/echo time = 40/11 ms; flip angle = 60°; matrix size = 512 × 128 × 32; field of view = 200 × 100 × 50 mm^3; total acquisition time = 2 min 44 s). The data sets were zero-filled in the two phase-encoding directions to equalize voxel sizes [$(0.39\ mm)^3$].

MRI Skeletal Rating

Skeletal age was independently rated from the MR images by two orthopedic specialists (raters A and B) who were blinded to the chronological age, according to the TW2-Japan RUS system (RUS stands for radius, ulna, and the 11 short bones in rays 1, 3, and 5; Ref. 12). Rater A rated the images twice after a two-week interval (A1 and A2). The correlation between chronological age and MRI skeletal age was determined by means of a simple linear regression analysis. Pearson's correlation coefficient (r) was used to measure inter-rater (A1 vs. B and A2 vs. B) and intrarater (A1 vs. A2) reproducibility.

Segmentation

The segmentation was performed to illustrate 3D skeletal features using ITK-SNAP (13) based on a level-set method. Prior to segmentation, an MR image was normalized such that the output image had a zero mean and a variance of one. In the preprocessing step of ITK-SNAP, the normalized image was converted into a probability map (lower threshold = 0.7–2.8; smoothness = 3.0). Several seeds were then manually placed in a bone to be segmented to initialize the active contour. Finally, the active contour evolution was computed using the probability map based on region competition (balloon force = 1.0; curvature force = 0.2–0.6). In regions where the bone boundaries were ambiguous, manual segmentation was carefully performed on a slice-by-slice basis. The segmented images were not used for MRI skeletal rating, because the current segmentation process is very time consuming.

FIG. 1. Overview of an open, compact MRI system and an example of hand imaging of a volunteer. [Color figure can be viewed in the online issue, which is available at wileyonlinelibrary.com.]

RESULTS

MR Images

All the volunteers were relaxed during the MR examination, and MR images were obtained for all of them. Figure 2a–c shows MR images of the left hand and wrist of the second-youngest volunteer (A). Small bones were visible in the MR images. For example, the small hamate (with a volume of 222 mm^3) was clearly distinguishable in the coronal and axial images, as indicated by the yellow arrows. As shown in the magnified images of the coronal sections (Fig. 1), the morphological features of the epiphyses of short bones in ray 1 (red arrows) can also be easily discriminated. Figure 2d shows a 3D view of segmented bones, which illustrates the detailed structures of the epiphyses used for skeletal assessment (sketched in yellow in Fig. 2d) as well as those of the diaphyses and carpal bones (sketched in white). Figure 3 shows another example of MR images and 3D segmentation obtained from an older volunteer (B).

MRI Skeletal Assessment

The developmental status of individual bones and epiphyses were judged on the basis of TW2 maturity indicators visible in the MR images. Examples of the maturity indicators were as follows. The distal epiphysis of the radius (white arrows in Fig. 3) began to form palmar and dorsal surfaces for articulation. The epiphysis of the distal phalanx of the thumb (red arrows) showed the formation of the saddle. That of the proximal phalanx (blue arrows) was wider than its diaphysis, and its articular facet was slightly concave. That of the metacarpal (pink arrows) was wider than its articular facet. These crucial markers are indicative of certain age demarcations.

Figure 4 shows an example of skeletal assessment of the distal epiphysis of the radius, which represents 20% of the total score. The radius has nine TW2

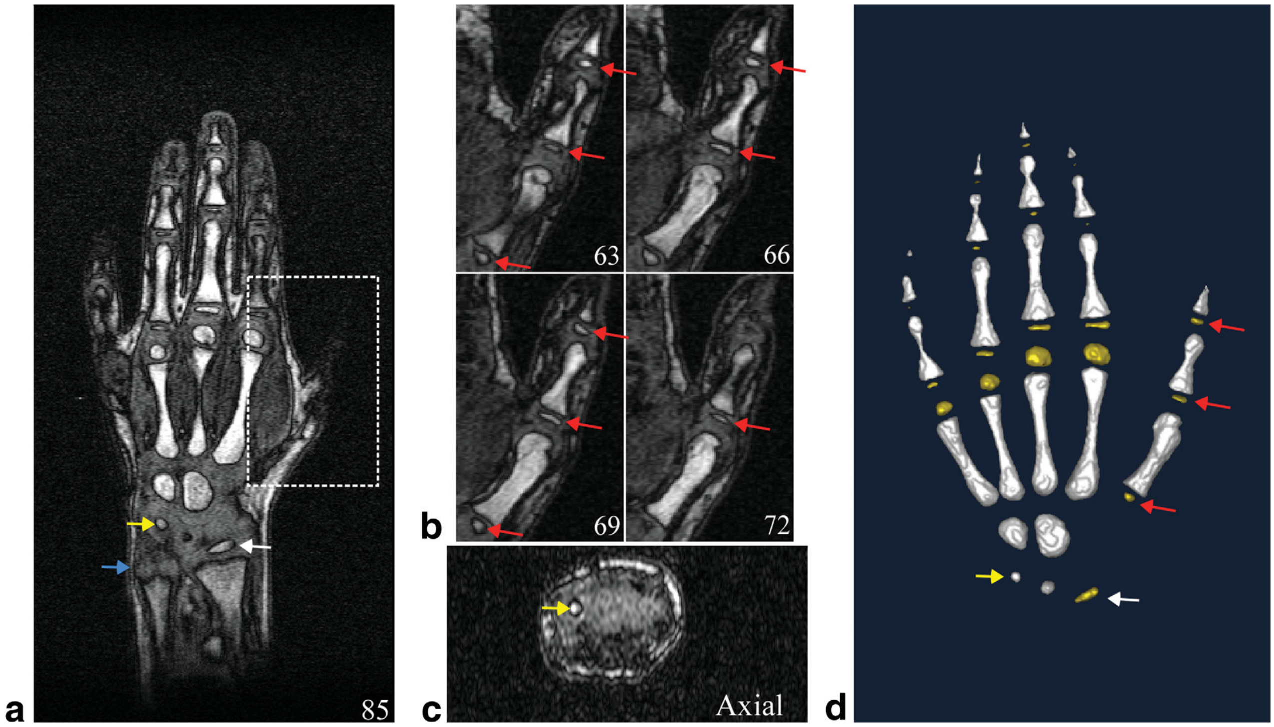

FIG. 2. MR images and segmented bones of the left hand of a healthy 5.1-year-old boy (volunteer A). **a**: Coronal section of the whole hand. **b**: Magnified view of coronal sections near the thumb. The figure in each image is the slice number. **c**: Axial selection near the wrist. **d**: 3D view of segmented bones. In each image, the hamate, epiphysis of radius, and epiphyses of short bones in ray 1 are indicated by the yellow, white, and red arrows, respectively. The blue arrow in (a) indicates the cartilaginous epiphysis of the ulna. The bones used for MR rating are sketched in yellow in (d). The segmented image was not used for MR rating.

developmental stages from A to I. The epiphysis is entirely cartilaginous at stage A, and begins to ossify and grows until it attains its definitive adult form. In this case, the stages from D to I were found. For example, the radius of volunteer A was assigned to be at the stage D where the epiphysis was comb-shaped, the third part of its proximal margin was flat, and its width was half or more than that of the metaphysis. Another intelligible example of a maturity indicator is a hump (surrounded by the squares) in stage G, capping in stage H (surrounded by the circles), and the fusion in the stage I, all of which were clearly visible in the MR images in Figure 4.

MRI Skeletal Rating

Eighty-three out of 93 cases were rated. Four cases (age range = 5.3–9.1 years; mean = 6.9 years) were excluded because of a severe motion artifact, and six cases (age range = 13.2–15.8 years; mean = 14.4 years) could not be evaluated, because the distal phalangeal joint was out of the field of view or demonstrated significant signal loss.

Figure 5a shows MRI skeletal age as a function of chronological age. This shows a strong positive linear correlation between the MRI skeletal age and chronological age (r = 0.921, 0.909, and 0.866 for raters A1, A2, and B, respectively). The intrarater reliability was high (r = 0.958 (A1 vs. A2)). The inter-rater reliability was also high (r = 0.922 (A1 vs. B) and 0.926 (A2 vs. B)). All correlations were highly significant ($P < 0.0001$).

Stage disagreement was defined as two or more stage differences for each bone between raters A1, A2, and B. Stage disagreement was most frequently found in the ulna and fifth metacarpal bone (Fig. 5). However, there was no significant correlation between the chronological age and the number of stage disagreements.

DISCUSSION

First, we discuss the validity of the MRI-based skeletal age assessment. In this study, despite the limited measurement time (2 min 44 s) to avoid unfavorable motion, the signal-to-noise ratio was sufficiently high (typically ~25) to resolve each bone and discriminate the detailed morphological structures. The maturity indicators necessary for the conventional TW2 skeletal assessment, such as formation of the hump, saddle, and concave surface, the appearance of capping and fusion, and the difference in width between the metaphysis and epiphysis, could be judged precisely from the MR images. This enables reliable MR rating of skeletal age. Indeed, the correlation between the skeletal and chronological ages was high and significant. Furthermore, the intrarater and inter-rater reproducibility was high. These results demonstrate the validity and reliability of the skeletal age assessment using MRI.

Stage disagreement between raters, which was defined in this study as two or more stage differences for each bone between raters, was more often seen in the ulna, radius, first metacarpal, and fifth distal phalanx. These bones were imaged close to the edge of the field of view,

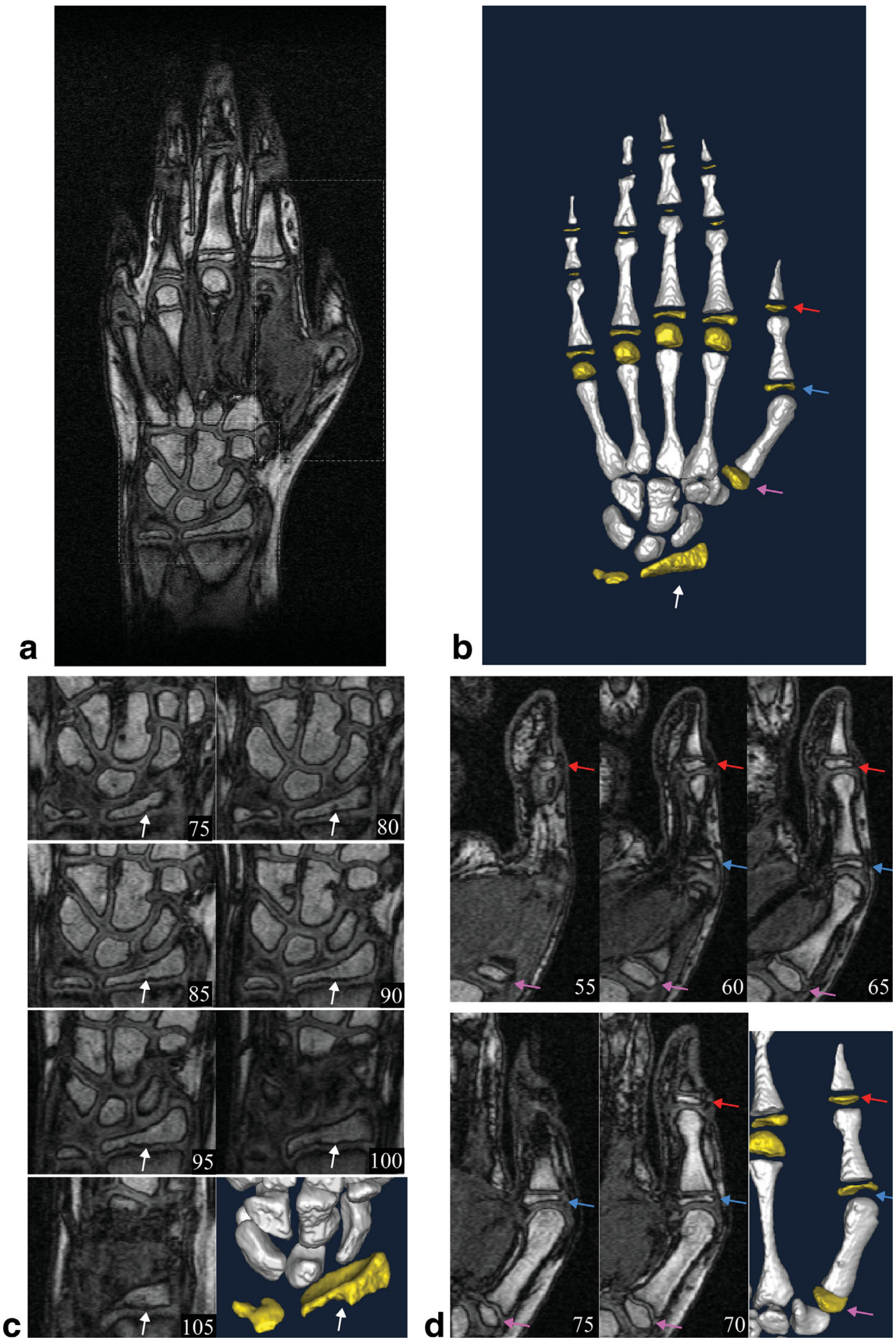

FIG. 3. MR images and segmented bones of the left hand of a healthy 10.2-year-old girl (volunteer B). **a**: Coronal section of the whole hand. **b**: 3D view of segmented bones. **c**,**d**: Magnified images of coronal sections near (c) the thumb and (d) the palm. The figure in each image is the slice number. In each image, the epiphyses of radius, the metacarpal, the proximal phalanx, and the distal phalanx in ray 1 are indicated by the white, pink, blue, and red arrows, respectively. The segmented image was not used for MR rating.

resulting in signal reduction. The resulting decrease in the signal-to-noise ratio complicates the MR rating, especially for small bones. More accurate rating could be achieved through uniform radiofrequency excitation. Another cause of the stage difference is that with the current sequence there is insufficient contrast between bone and cartilage, which might obscure clear delineation of the morphology of the small bones.

MRI has an advantage in having excellent soft tissue contrast with a multiplanar cross-sectional imaging capability. Cartilage is well visualized in MRI, and its growth assessment might provide additional important information on skeletal maturity during infancy. For example, the formation of the cartilaginous epiphysis of the ulna with no center of ossification was identified in Figure 2a (as indicated by the blue arrow). However, in some cases, the resolution (especially in the phase direction) was not high enough to bring out the signal contrast between cartilage and muscle. An additional pulse sequence with a short scan time such as a T_2^*-weighted sequence may have been more helpful to assess the high signal contrast of the cartilage.

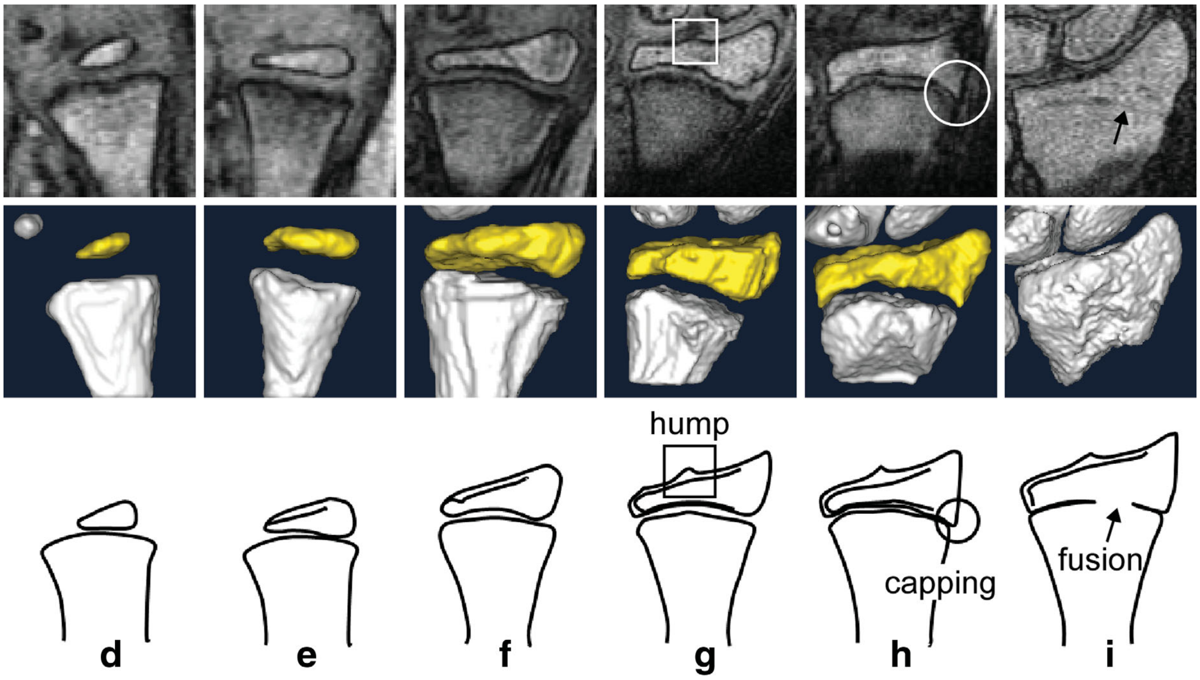

FIG. 4. Skeletal assessment of the distal epiphysis of the radius for TW2 stages from **d** to **i**. The chronological ages and sexes of each volunteer are (d) 5.1 (boy), (e) 4.2 (girl), (f) 9.9 (boy), (g) 11.5 (boy), (h) 14.0 (girl), and (i) 16.4 (boy). The schematic representations in the lower part were drawn according to Ref. 2. [Color figure can be viewed in the online issue, which is available at wileyonlinelibrary.com.]

The 3D capability of MRI allows more accurate assessment of skeletal age and maturity. For example, in the TW2 system, the formation of the articular facet is judged by the appearance of a white line (cortical line) in an X-ray file. Such a complicated morphological feature is more accurately assessable in 3D MR images, as shown in Figure 3c. 3D MRI capability also provides a new way to unveil novel maturity indicators, such as bone volumes. With a more sophisticated technique such as full automation of segmentation (14,15), MR volumetry of the bones would be a time-saving, robust, and reliable skeletal assessment.

Skeletal age has been used to evaluate bone growth speed, and maturation, which might be influenced by genetic, developmental, metabolic, and endocrinal diseases. Two papers regarding the relationship between childhood obesity and skeletal age have recently been published (16,17). Skeletal age measurement using MRI may become more important to assess childhood obesity.

There are several limitations in this study. First, some young children had difficulty keeping still during the examination, which resulted in a severe motion artifact, although the MR scan time was short. This is partly because the fixation of their hands and wrists was not sufficient. More stable fixation as well as parental support would be effective. The unfavorable motion could also be suppressed by shortening the scan time with the aid of, for example, partial Fourier acquisition (18–20). Second, the hands and wrists of some adolescents were too large to include the distal phalanx within the field of view. These grown-up children might be tolerant of a long measurement time, and this problem could be overcome by imaging the wrist and distal hand separately.

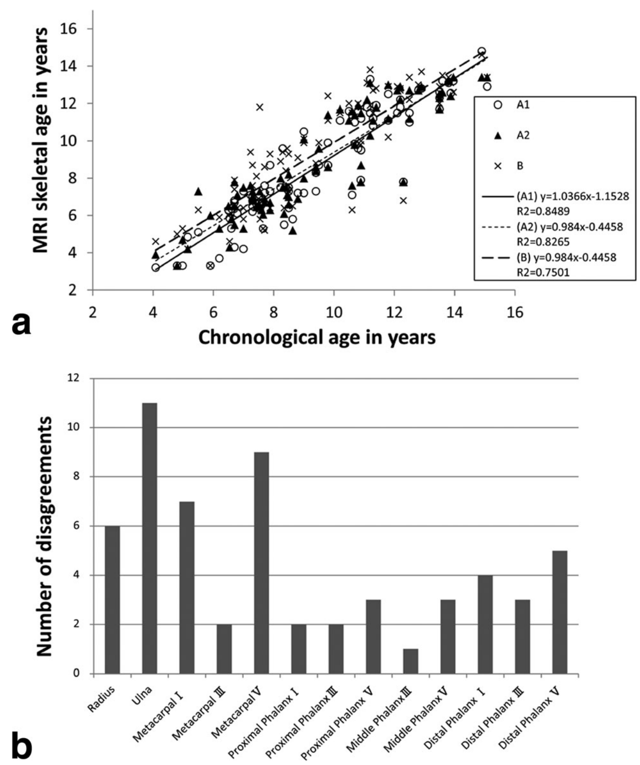

FIG. 5. Reliability of MRI skeletal assessment. **a**: Correlation between skeletal age assessed on the basis of MR rating and chronological age. **b**: Number of cases where two or more stage differences for each bone between raters A1, A2, and B were found.

Third, children younger than 4 years old were not included in this study. Finally, a radiographic atlas was used to assess skeletal age in MRI. An MRI skeletal age atlas would be necessary in the future. Despite these limitations, we believe an open, compact MRI system is a useful imaging tool for assessment of skeletal age.

The methodology presented in this study is applicable to conventional whole-body and extremity scanners. The use of a conventional wrist or extremity coil would provide high image quality to visualize small bones of young children. The sequence parameters should be determined to meet two requirements: a spatial resolution high enough to resolve small bones and a measurement time short enough not to cause discomfort and movement. The voxel size and the measurement time used in this study were $0.39 \times 0.78 \times 1.56$ mm^3 [(0.39 mm)^3 after the zero-filled process] and 2 min 44 s, respectively; these parameters could guide the sequence design. The sequences that meet these requirements are easily installable in conventional scanners.

In this study, the use of an open and compact scanner facilitated the realization of a comfortable environment for children. An equivalent environment might be realized for conventional tunnel-type scanners through the suitable positioning and parental support. The use of a wide and short scanner would also be helpful in preventing discomfort for the children. Overall, the findings of this study might lead to the development of a new standard for assessing skeletal maturation in children.

CONCLUSIONS

In this study, we gave an experimental demonstration of skeletal assessment using an open, compact MRI optimized for the imaging of a child's hand and wrist. MRI and 3D segmentation visualized the detailed morphological features of individual bones in the hand and wrist with a short scan time. The skeletal age based on MR ratings had a strong positive correlation with the chronological age and demonstrated high and significant intrarater and inter-rater reproducibility. These results demonstrate the validity and reliability of skeletal age assessment based on MRI. Our results indicate that MRI could be a powerful, noninvasive, and nonirradiative method for assessment of skeletal age and maturity in children.

REFERENCES

1. Acheson RM. A method of assessing skeletal maturity from radiographs; a report from the Oxford child health survey. J Anat 1954;88:498–508.
2. Bertaina C, Stasiowska B, Benso A, Vannelli S. Is TW3 height prediction more accurate than TW2? Preliminary data. Horm Res 2007;67:220–223.
3. Greulich WW, Pyle SI. Radiographic atlas of skeletal development of the hand and wrist, 2nd ed. Stanford, CA: Stanford University Press; 1959.
4. Tanner JM. Assessment of skeletal maturity and prediction of adult height (TW2 method), 2nd ed. London; New York: Academic Press; 1983.
5. Bilgili Y, Hizel S, Kara SA, Sanli C, Erdal HH, Altinok D. Accuracy of skeletal age assessment in children from birth to 6 years of age with the ultrasonographic version of the Greulich-Pyle atlas. J Ultrasound Med 2003;22:683–690.
6. Dvorak J, George J, Junge A, Hodler J. Age determination by magnetic resonance imaging of the wrist in adolescent male football players. Br J Sports Med 2007;41:45–52.
7. George J, Nagendran J, Azmi K. Comparison study of growth plate fusion using MRI versus plain radiographs as used in age determination for exclusion of overaged football players. Br J Sports Med 2012;46:273–278.
8. Dvorak J, George J, Junge A, Hodler J. Application of MRI of the wrist for age determination in international U-17 soccer competitions. Br J Sports Med 2007;41:497–500.
9. Handa S, Haishi T, Kose K. Development of a local electromagnetic shielding for an extremity magnetic resonance imaging system. Rev Sci Instrum 2008;79:113706.
10. Yoshioka H, Ito S, Handa S, Tomiha S, Kose K, Haishi T, Tsutsumi A, Sumida T. Low-field compact magnetic resonance imaging system for the hand and wrist in rheumatoid arthritis. J Magn Reson Imaging 2006;23:370–376.
11. Suzuki T, Ito S, Handa S, et al. New low-field extremity MRI, compacTscan; comparison with whole-body 1.5T conventioanl MRI. Mod Rheumatol 2010;20; 331–336.
12. Japanese Society for Pediatric Endocrinology & The Japanese Association for Human Auxology eds. AosafJc, Medical View, Tokyo, Japan; 2011 (in Japanese).
13. Yushkevich PA, Piven J, Hazlett HC, Smith RG, Ho S, Gee JC, Gerig G. User-guided 3D active contour segmentation of anatomical structures: significantly improved efficiency and reliability. NeuroImage 2006;31:1116–1128.
14. Lemieux L, Hagemann G, Krakow K, Woermann FG. Fast, accurate, and reproducible automatic segmentation of the brain in T1-weighted volume MRI data. Magn Reson Med 1999;42:127–135.
15. Morra JH, Tu Z, Apostolova LG, et al. Validation of a fully automated 3D hippocampal segmentation method using subjects with Alzheimer's disease mild cognitive impairment, and elderly controls. NeuroImage 2008;43:59–68.
16. Sopher AB, Jean AM, Zwany SK, Winston DM, Pomeranz CB, Bell JJ, McMahan DJ, Hassoun A, Fennoy I, Oberfield SE. Bone age advancement in prepubertal children with obesity and premature adrenarche: possible potentiating factors. Obesity 2011;19:1259–1264.
17. Johnson W, Stovitz SD, Choh AC, Czerwinski SA, Towne B, Demerath EW. Patterns of linear growth and skeletal maturation from birth to 18 years of age in overweight young adults. Int J Obesity 2012;36:535–541.
18. Liang Z-P, Boada FE, Constable RT, Haacke EM, Lauterbur PC, Smith MR. Constrained reconstruction methods in MR imaging. Rev Magn Reson Med 1992;4:67–185.
19. McGibney G, Smith MR, Nichols ST, Crawley A. Quantitative evaluation of several partial Fourier reconstruction algorithms used in MRI. Magn Reson Med 1993;30:51–59.
20. Noll DC, Nishimura DG, Macovski A. Homodyne detection in magnetic resonance imaging. IEEE T Med Imaging 1991;10:154–163.